Electron energy loss near supported particles

N. Zabala
Departamento Electricidad y Electrónica, Facultad de Ciencias, Universidad del País Vasco-Euskal Herriko Unibertsitatea, Apartado 644, 48080 Bilbao, Spain

A. Rivacoba
Departamento Física de Materiales, Facultad de Química, Universidad del País Vasco-Euskal Herriko Unibertsitatea, Apartado 1072, 280080 San Sebastian, Spain
(Received 7 May 1993)

A general expression for the energy-loss probability in scanning transmission electron microscopy valid for complex microstructures is presented in the framework of classical dielectric theory. Calculations are carried out for small particles half embedded in a planar interface. We used experimental data for the dielectric functions that characterize the media and we take into account the coupling among different multipolar terms. Resonances, present neither in the planar-interface nor in the isolated-sphere energy-loss spectra, are found. The results agree with many experimental results reported in the literature of the last few years. A different behavior between conducting and insulator supports is found. The effect of an oxide coating around the spherical particle is also discussed.

I. INTRODUCTION

In the last decade, electron-energy-loss spectroscopy (EELS) in scanning transmission electron microscopy (STEM) has become a useful tool in the study of microstructural systems such as catalysts or semiconductor devices. The first EELS experiments with small particles (of 10–100 nm) using an extended electron beam were performed by Fujimoto and Komaki.[1,2] With the development of the STEM microscope it has been possible to use focused beams of around 0.5-nm width and 100-KeV energy. With these conditions, Batson[3,4] performed experiments varying the probe impact parameter across small particles. The classical dielectric theory has been proved to describe successfully those experiments.[5,6] Ferrell and Echenique[7] obtained an expression of the energy-loss probability that contains many multipolar terms and allows use of the experimental dielectric functions to characterize the sphere and the surrounding medium. Echenique, Bausells, and Rivacoba[8] used a self-energy treatment to obtain the energy-loss probability in small spheres, including also the case of penetrating trajectories. In most experimental situations, the small metallic particles appear covered with an oxide layer of a few nanometers. The influence of an oxide layer has been extensively studied in the literature;[9–13] it causes a displacement of the surface plasmon excitation toward lower energies as the oxide thickness increases. The model has been extended to consider nonlocal dielectric functions to characterize the different media of the target.[14–20]

In the aforementioned works, small particles have been considered as isolated spheres immersed in an infinite medium. Nevertheless, this approximation seems to be insufficient to describe some experiments in which the particles appear in clusters or partially embedded in a matrix of another material. Batson[10,21] observed anomalous peaks in the region of 2–5 eV in the energy-loss spectrum of fast electrons in 10–50-nm oxide-coated Al spheres that he attributed to the interaction of two neighboring spheres. Ugarte and co-workers[27–29] also reported a 3–4-eV excitation surface mode in Si-oxidized particles, not predicted by the one-layer, oxide-coated, sphere model, that they interpreted with the introduction of a second ultrathin (of around 0.5 nm) conducting layer. As has been reported in the literature, small Al particles can be obtained by irradiating AlF_3 films with the STEM microscope.[25] Howie and Walsh[26] have studied systems of Al small particles in a matrix of AlF_3, and studied them in terms of dielectric excitation theory for a two-phase medium. They find that even the most sophisticated effective-medium theories available[27,28] are not quite successful in explaining their energy-loss spectra. They obtain a better fit to their observations by considering an effective loss function that is an average over different parts of typical trajectories in the complex medium. As they state, the development of that theory would allow its applicability to a wide range of microstructural problems. Wang and Cowley[29–32] have reported an extended experimental study on the effect of different supports on the energy-loss spectra in Al particles.

Different attempts have been done in the literature to extend the theoretical models to those situations of mixed geometries such as, for example, systems of two spheres,[21,33–34] two cylinders,[35] or a sphere-plane system.[36,29–32] In many of those works the surface modes in such kind of systems have been studied avoiding the coupling between different multipolar terms.[21,33,36] Nevertheless, that approach is not valid when the different components of the system are very close or interpenetrate. Wang and Cowley studied the sphere-plane system when the sphere is half embedded in the support, but their theoretical approach is unsatisfactory insofar as they mix time and frequency in solving the Poisson equa-

tion. From their derivation of the energy-loss probability, they are not able to recover the single-surface limits.

In this work, a general formalism to calculate the energy-loss probability valid for a wide range of experimental STEM situations is presented first. The expression so obtained is applied to the problem of a small particle coupled to a planar interface (half embedded in it). Experimental optical data for the complex dielectric functions $\varepsilon(\omega)$ are used to characterize the different media, in order to obtain good fitting with the experimental results available. Special emphasis is placed on the corrections introduced in the loss probability spectrum by the presence of the support. From our expressions, the energy-loss probability of the isolated sphere is obtained as the particular case which occurs when the dielectric functions of the two media around the particle become the same. Different cases of particular experimental interest are considered, as aluminum or silicon particles in different supporting media. The effect of the oxide coating around the particle on the energy-loss probability is studied, as well.

II. GENERAL DIELECTRIC FORMALISM

In this section we introduce a general formalism to calculate the energy-loss probability of a moving point charge in the framework of dielectric theory. The target is described by a set of local dielectric functions $\varepsilon_i(\omega)$. An advantage of the following formalism is that the expressions obtained are available for any local dielectric response function, so that experimental data can be used in the computations. Nonlocal effects have been found to be relevant at probe-surface distances smaller than about 1 Å.[37] Therefore, our approach is valid for trajectories in which the electron expends most of the time at distances larger than 1 Å from the interface. In the following, all the equations are expressed in atomic units.

The interaction between the electron and the target is given by the induced potential, that is the solution of the Poisson equation where the direct Coulombian term has been removed. In Fourier ω space the total potential is given by

$$\nabla^2\Phi(\mathbf{r},\omega)=-\frac{4\pi}{\varepsilon(\omega)}\rho(\mathbf{r},\omega)\ , \tag{1}$$

where $\rho(\mathbf{r},\omega)$ is the charge density in the ω space. The problem can also be described in terms of the screened interaction $W(\mathbf{r},\mathbf{r}',\omega)$, i.e., the solution of Eq. (1) for a point electron at rest at $\mathbf{r}'$. Then that function satisfies the Green's equation

$$\nabla^2 W(\mathbf{r},\mathbf{r}',\omega)=-\frac{4\pi}{\varepsilon(\omega)}\delta(\mathbf{r}-\mathbf{r}')\ . \tag{2}$$

The solution of the particular electrostaticlike problem is obtained by matching the boundary conditions at the different limiting interfaces, that is the continuity of the potential and the normal component of the displacement field.

In most STEM situations the probe electron can be considered as moving with velocity $\mathbf{v}$ parallel to the x axis. Then its trajectory is given by $\mathbf{r}=(x=vt,b_y,b_z)$, and the ω component of its charge density is

$$\rho(\mathbf{r},\omega)=-\frac{1}{v}e^{i\omega x/v}\delta(y-b_y)\delta(z-b_z)\ . \tag{3}$$

The magnitude involved in the calculation of the energy loss of the electron is just the induced part of the total potential. In terms of the induced part of the screened interaction, it is obtained as follows:

$$\Phi^{\mathrm{ind}}(\mathbf{r},t)=-\frac{1}{2\pi v}\left[\int_{-\infty}^{+\infty}d\omega\int_{-\infty}^{+\infty}dx'e^{-i\omega(t-x'/v)}W^{\mathrm{ind}}(\mathbf{r},\mathbf{r}',\omega)\right]_{\mathrm{traj}}\ , \tag{4}$$

where $\mathbf{r}'$ in W^{ind} is evaluated at the trajectory, i.e., $y'=b_y$ and $z'=b_z$. The total-energy loss can be calculated as the work developed against the retarding electric field acting on the electron along the whole trajectory:

$$W=\int_{-\infty}^{+\infty}\left[\frac{\partial\Phi^{\mathrm{ind}}}{\partial x}\right]_{\mathrm{traj}}dx$$
$$=\int_{-\infty}^{+\infty}(d\Phi^{\mathrm{ind}})_{\mathrm{traj}}-\int_{-\infty}^{+\infty}\left[\frac{\partial\Phi^{\mathrm{ind}}}{\partial t}\right]_{\mathrm{traj}}dt\ , \tag{5}$$

where the derivatives of the potential are evaluated at the trajectory $(t=x/v,y=b_y,z=b_z)$. In many cases of interest, Eq. (5) becomes

$$W=-\frac{1}{v}\int_{-\infty}^{+\infty}\left[\frac{\partial\Phi^{\mathrm{ind}}}{\partial t}\right]_{\mathrm{traj}}dx\ , \tag{6}$$

since when the induced potential is the same at both ends of the trajectory, i.e., $\Phi^{\mathrm{ind}}(x=-\infty)=\Phi^{\mathrm{ind}}(x=+\infty)$, the integration in Φ^{ind} in the right-hand side of expression (5) annulates. Then, if the total energy loss is expressed in terms of the energy-loss probability $P(\omega)$ as usual,

$$W=\int_0^{+\infty}d\omega\,\omega P(\omega) \tag{7}$$

and taking into account the properties of parity with respect to ω fulfilled by $\varepsilon(\omega)$ and $W(\mathbf{r},\mathbf{r}',\omega)$, the energy-loss probability is given by the following double integral along the electron's trajectory:

$$P(\omega)=\frac{1}{\pi v^2}\int_{-\infty}^{+\infty}dx'\int_{-\infty}^{+\infty}dx\ \mathrm{Im}\{W^{\mathrm{ind}}(\mathbf{r},\mathbf{r}',\omega)\times e^{-i\omega(x-x')/v}\}\ , \tag{8}$$

where both $\mathbf{r}$ and $\mathbf{r}'$ are evaluated at the trajectory. This last condition can be incorporated by means of Eq. (3). Then the meaning of $P(\omega)$ is more clear when expressed in terms of the charge density:

$$P(\omega)=\frac{1}{\pi}\int_{-\infty}^{+\infty}d\mathbf{r}'\int_{-\infty}^{+\infty}d\mathbf{r}\ \mathrm{Im}\{\rho^*(\mathbf{r},\omega)W^{\mathrm{ind}}(\mathbf{r},r',\omega)\times\rho(\mathbf{r}',\omega)\}\ , \tag{9}$$

where ρ^* means the complex conjugate of ρ. In this way, the energy-loss probability can be understood as the average value of the imaginary part of the screened interaction over the whole trajectory. Furthermore, Eq. (9) has a wider range of applicability; it is not just restricted to the special trajectory considered in our problem, as it is the case of Eq. (8).

Note that the validity of both Eqs. (8) and (9) is restricted to those situations which occur when the previously mentioned condition for the induced potential is applicable. That condition can be better understood in the framework of the time-dependent perturbation theory.[38] In this way, one avoids the elastic contributions to the energy loss, which vanish when considering the whole trajectory. That is trivially fulfilled in the case of finite targets, since the potential then annulates at both extremes of the trajectory. The condition holds for infinite targets as well whenever the initial and final probe-target state is the same. For instance, in the case of a planar interface, the previous expressions remain valid for trajectories parallel to the plane (or for the case of specular reflection), but they are not applicable to penetrating trajectories. The known expressions for films in normal incidence[39] and for isolated particles[7–9] are recovered from ours, as is to be expected. This allows the application of expression (8) for calculating the energy-loss probability in complex structures such as small particles supported in a large planar interface (as is discussed in Sec. II A). On the other hand, it should be noticed that, for finite targets, the model allows calculation of the energy loss due to the whole trajectory (which is just the magnitude measured in the EELS analyzer), and does not give the stopping power at different trajectory points. Nevertheless, in the case of an electron moving parallel to a planar or cylindrical interface (where the condition is fulfilled at any point of the trajectory) the well-known expressions of the stopping power[40–43] are straightforwardly obtained. In the self-energy formalism, considering well-focused beams and neglecting the recoil of the probe, the same expression (8) is obtained.[44] In that treatment[45,46] the energy-loss probability is related to the energy-loss rate γ experienced by the particle, which in turn is given in terms of the imaginary part of the incident electron self-energy Σ_0 by $\gamma=-2\,\mathrm{Im}(\Sigma_0)$. There, the self-energy is written in terms of the Green's function and the screened interaction $W(\mathbf{r},\mathbf{r}',\omega)$, and the electron is described by a wave packet. The connection between classical and quantal models was first pointed out by Ritchie[47] and Ritchie and Howie.[48]

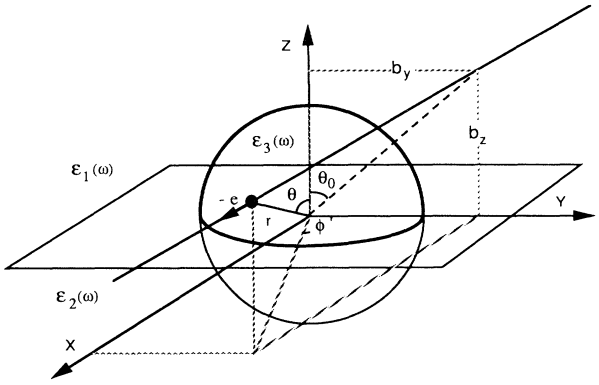

FIG. 1. Electron traveling near a half-embedded sphere. The trajectory is defined by $x=vt$, $y=b_y$ and $z=b_z$. The spherical coordinates r, ϕ, and $\mu=\cos\theta$ used to solve the problem are also indicated. The different media are characterized by the local dielectric functions $\varepsilon_1(\omega)$, $\varepsilon_2(\omega)$, and $\varepsilon_3(\omega)$.

To illustrate the application of the models, we examine below the case of a spherical particle coupled to a planar interface.

A. Small particle coupled to a planar interface: Half-embedded particle

The previous treatment is general, allowing application to different geometries, but now we restrict the analysis to the particular geometry sketched in Fig. 1. This geometry represents the common experimental situation in which the particle is supported by a large surface. The dielectric response functions of the particle and the surrounding media are $\varepsilon_3(\omega)$, $\varepsilon_1(\omega)$, and $\varepsilon_2(\omega)$, respectively. The applicability of Eq. (8) to this case is ensured since the electron trajectory is parallel to the interface, and the initial and final electron-plane system states remain invariant, as explained above. We consider trajectories in the upper medium parallel to the interface and external to the particle. The problem of trajectories penetrating the particle also can be studied by this method. To solve the electrostaticlike problem, we write first the screened interaction functions $W(\mathbf{r},\mathbf{r}',\omega)$ at the three media. In the region external to the small particle, we write the solution as one part corresponding to the planar interface (image charges), plus the appropriate multipolar expansion to yield the effect of the small particle:[49]

$$W_1(\mathbf{r},\mathbf{r}',\omega)=-\frac{1}{\varepsilon_1}\frac{1}{|\mathbf{r}-\mathbf{r}'|}-\frac{1}{\varepsilon_1}\frac{\varepsilon_1-\varepsilon_2}{\varepsilon_1+\varepsilon_2}\frac{1}{|\mathbf{r}-\mathbf{r}''|}+\sum_{l=0}^{\infty}\sum_{m=-l}^{l}A_{lm}\frac{a^l}{r^{l+1}}P_{lm}(\mu)e^{im(\phi-\phi')}\quad\left[r\geq a\ ,\ 0\leq\theta\leq\frac{\pi}{2}\right],$$

$$W_2(\mathbf{r},\mathbf{r}',\omega)=-\frac{2}{\varepsilon_1+\varepsilon_2}\frac{1}{|\mathbf{r}-\mathbf{r}'|}+\sum_{l=0}^{\infty}\sum_{m=-l}^{l}B_{lm}\frac{a^l}{r^{l+1}}P_{lm}(\mu)e^{im(\phi-\phi')}\quad\left[r\geq a\ ,\ \frac{\pi}{2}\leq\theta\leq\pi\right],\tag{10}$$

$$W_3(\mathbf{r},\mathbf{r}',\omega)=\sum_{l=0}^{\infty}\sum_{m=-l}^{l}C_{lm}\frac{r^l}{a^{l+1}}P_{lm}(\mu)e^{im(\phi-\phi')}\quad(r\leq a\ ,\ 0\leq\theta\leq\pi)\ .$$

$\mathbf{r}'=(r',\theta',\phi')$ denotes the electron position in spherical coordinates, $\mathbf{r}''=(r',\pi-\theta',\phi')$ that of its image with respect to

the plane, and $\mu=\cos\theta$. The advantage of this procedure is that now the boundary conditions on the plane must be matched only with the multipolar series, as the image charge fulfill them trivially. After doing so, the following relation is obtained between the coefficients:

$$B_{lm}=\eta_{lm}A_{lm}\ , \tag{11}$$

with

$$\eta_{lm}=\begin{cases}1\ , & l+m \text{ even}\\ \varepsilon_2/\varepsilon_1, & l+m \text{ odd}\ .\end{cases}$$

When matching the boundary conditions on the spherical surface $r=a$, for $\theta\leq\pi/2$ and $\theta\geq\pi/2$, a set of systems of linear equations (one for each value of $m\geq 0$) is obtained for the coefficients A_{lm}:

$$\frac{2}{\varepsilon_1+\varepsilon_2}\sum_l d_{lm}[(\varepsilon_1 l-\varepsilon_3 j)\eta_{lm}+(-1)^{l+j}(l\varepsilon_2-j\varepsilon_3)]M_{lj}^m\left[\frac{a}{r'}\right]^{l+1}P_{lm}(\mu')$$
$$=\sum_l A_{lm}\left\{\varepsilon_1(l+1)+\varepsilon_3 j+\frac{(-1)^{l+j}}{\eta_{lm}}[(l+1)\varepsilon_2+j\varepsilon_3]\right\}M_{lj}^m\ , \tag{12}$$

for j and $l=m,\ldots,\infty$. Here

$$d_{lm}=\frac{(l-m)!}{(l+m)!}\ . \tag{13}$$

The elements of matrix M_{lj}^m are the following integrals of Legendre functions products:

$$M_{lj}^m=\int_0^1 P_{lm}(\mu)P_{jm}(\mu)d\mu\ . \tag{14}$$

Numerical values of those integrals can be found in the literature,[50,51] for $l+j$ even. Then they become $M_{lj}^m=[\delta_{jl}/(2l+1)][(l+m)!/(l-m)!]$, where δ_{jl} is the Kronecker delta. For $l+j$ odd, the integrals must be numerically computed. A fast way of computing these integrals by using the recurrence relations among the Legendre functions has been reported.[52]

As it is deduced from expression (12), the collective modes of the sphere-support system involve all the multipolar terms; they cannot be associated to one particular multipolar term, i.e., to an integer index, as in the case of an isolated sphere.

The energy-loss probability makes two contributions: one corresponding to the second term on the right-hand side of W_l in Eq. (10) (leading to the known expression of the stopping power of a particle moving near a planar interface[40]), and another related to the third term (with coefficients A_{lm}) that contains the contribution of the small particle to the potential. In the following, we concentrate on the second contribution to the energy-loss probability (derived from the A_{lm} terms). Then the energy-loss probability along the whole trajectory due to the embedded particle is expressed as

$$P(\omega)=\frac{2}{\pi v^2}\sum_{l=0}^{\infty}\sum_{m=0}^{l}\int_0^{\infty}dx\int_0^{\infty}dx'(2-\delta_{m0})\mathrm{Im}(A_{lm})\left\{\cos[m(\phi-\phi')]\cos\left[\frac{\omega}{v}(x-x')\right]\right.$$
$$\left.+\cos[m(\phi+\phi')]\cos\left[\frac{\omega}{v}(x+x')\right]\right\}\frac{a^l}{r^{l+1}}P_{lm}(\mu)\ , \tag{15}$$

where the coefficients A_{lm} are solutions of system (12), and the integrals are performed along the electron's trajectory, given by the spherical coordinates

$$r(x)=\sqrt{x^2+b_y^2+b_z^2},\quad \cos\theta=\mu(x)=\frac{b_z}{\sqrt{x^2+b_y^2+b_z^2}}\ ,\quad \phi(x)=\arctan\left[\frac{x}{b_y}\right]\ . \tag{16}$$

To write expression (15), the parity of coefficients A_{lm} and variables (16) with respect to x has been taken into account, allowing reduction of the integration interval to one half of the trajectory.

The energy-loss probability for an isolated sphere[7] is recovered from expression (15) if $\varepsilon_1=\varepsilon_2$ in the set of equations (12) that must fulfill the coefficients A_{lm}. When doing so, only the terms $l=j$ contribute to the summation, and functions $W_l(\mathbf{r},\mathbf{r}',\omega)$ and $W_2(\mathbf{r},\mathbf{r}',\omega)$ in expression (10) become equal.

B. Coated half-embedded particle

In some experimental situations the small particles present an external coating. A more realistic model is then to consider the case shown in Fig. 7. This problem can be solved in the manner of the Sec. II A. The coating layer intro-

duced is characterized by a dielectric function denoted by $\varepsilon_4(\omega)$. In this case the loss probability is formally given by the same expression (15) as for the clean sphere. The coefficients A_{lm} are now the solution of the following set of linear equations:

$$\frac{2}{\varepsilon_1+\varepsilon_2}\sum_l d_{lm}\{l(1+\alpha_j)[\varepsilon_1\eta_{lm}+(-1)^{l+j}\varepsilon_2]-\varepsilon_4[j-(j+1)\alpha_j][\eta_{lm}+(-1)^{l+j}]\}M_{lj}^m\left[\frac{a}{r'}\right]^{l+1}P_{lm}(\mu')$$
$$=\sum_l A_{lm}\{(l+1)(1+\alpha_j)\}\left[\varepsilon_1+(-1)^{l+j}\frac{\varepsilon_2}{\eta_{lm}}\right]+\varepsilon_4[j-(j+1)\alpha_j]\left[1+\frac{(-1)^{l+j}}{\eta_{lm}}\right]M_{lj}^m, \quad (17)$$

where

$$\alpha_j=\frac{j(\varepsilon_4-\varepsilon_3)}{j\varepsilon_3+(j+1)\varepsilon_4}\left[\frac{a_1}{a_2}\right]^{2j+1}, \quad (18)$$

and a_1 and a_2 are the coating internal and external radii, respectively.

Note that when $\varepsilon_3=\varepsilon_4$ in the previous expressions, $\alpha_j=0$ and Eqs. (17) become the same as (12), recovering thereby the expression of the loss probability for the single half embedded sphere. On the other hand, if $\varepsilon_1=\varepsilon_2$, the expression of the loss probability for an isolated oxidized sphere[9,11–13] is recovered.

III. NUMERICAL RESULTS AND COMPARISON WITH EXPERIMENTS

To evaluate the energy-loss probability $P(\omega)$ given by (15), the first step is to calculate the A_{lm} coefficients given by the solution of system (12), for each value of l and m and at each point of the electron's trajectory. In the following computations we have considered the contribution of the first 20 l terms in probability (15), but when solving the systems of Eqs. (12) or (17) to compute the A_{lm} coefficients we have considered the first 100 terms to ensure the convergence of the multipolar expansion. It is known in the case of the isolated particle that the number of terms necessary to ensure the convergence depends on the relative probe-target position.[5] When the electron is closer to the interface, especially in the planar case, more terms have to be included. The electron energy considered in all the calculations is 100 KeV.

In Fig. 2 we present the contribution to the energy-loss spectrum of the Al sphere half embedded in a support of the same material. In this case we have considered the Drude dielectric function for Al with a small damping constant ($\omega_p=15.1$ eV and $\gamma=0.27$ eV). We have calculated the spectra for different electron trajectories parallel to the planar interface, one passing over the top of the particle [$\theta_0=\arctan(b_y/b_z)=0$], denoted by A [Fig. 2(a)], and another two [Fig. 2(b)] for $\theta_0\neq 0$, denoted by B and C, for the same distance to the center of the sphere, $b(b=\sqrt{b_y^2+b_z^2})$. The radius of the spherical particle is $a=10$ nm and the impact parameter is $b=11$ nm. In Fig. 2(a) we have also plotted the spectra corresponding to the isolated sphere (dotted line) of the same radius and the Al-vacuum planar interface for a trajectory length of $2a$ (dashed line). It must be stressed that the spectra have been calculated from (15), where only the sphere contribution to the energy-loss probability, as given by the A_{lm} terms in (10), has been taken into account. That explains why the spectrum becomes negative around $\omega_s=\omega_p/\sqrt{2}$ (i.e., 10.7 eV for aluminum), which is the surface plasmon energy in the planar interface. Furthermore, as it can be noticed in Fig. 2(a), the intensity of the negative peak corresponds just to a trajectory length of $2a$ (the particle diameter) near an infinite planar interface. This suggests

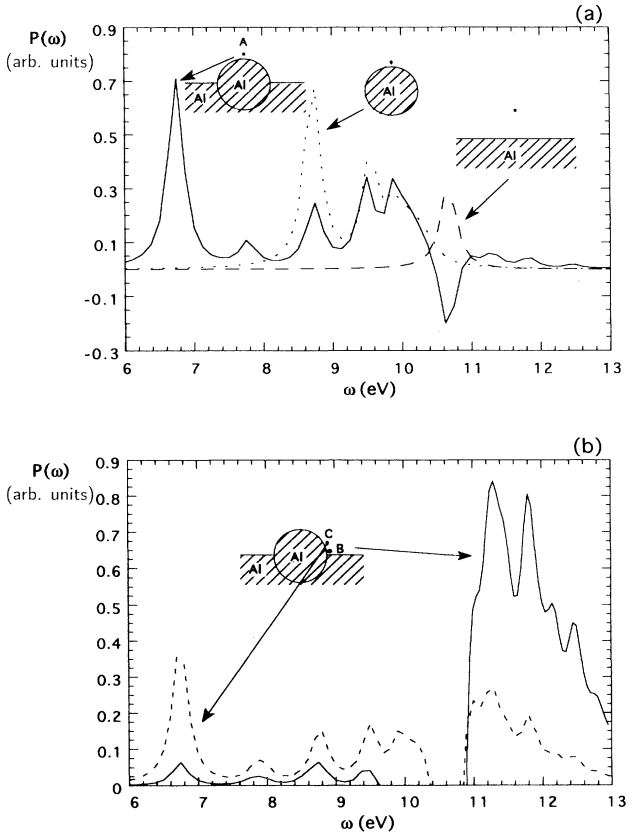

FIG. 2. (a) Calculated spectra corresponding to an Al sphere of radius $a=10$ nm half embedded in an Al-vacuum interface (continuous line). The electron trajectory (A) shown in the scheme corresponds to $\theta_0=0$ and $b=11$ nm. Spectra corresponding to the same impact parameter near an isolated sphere (dotted line) and a planar interface for length $2a$ (dashed line) have also been plotted. (b) Calculated energy-loss spectra for an Al sphere of radius $a=10$ nm supported in an Al-vacuum interface and impact parameter $b=11$ nm. The probe trajectory B (continuous line) corresponds to $\theta_0=85°$, and C (dashed line) to $\theta_0=60°$.

that one effect of the particle is to introduce a correction in the spectrum for a planar interface: a decrease in the loss probability of an infinite plane due to the presence of the small particle. In any case, when adding the energy loss corresponding to the planar interface, which has a maximum at $\omega_s=\omega_p/\sqrt{2}$ (i.e., 10.7 eV for aluminum), this point is resolved, and the total probability becomes positive in that range. On the other hand, it can be noticed that in the range 8–10 eV, the spectrum looks like that of an isolated sphere, except that the intensity of the dipolar term has been relatively reduced. Thus the structure of the spectrum can be interpreted as a superposition of the spectra corresponding to both constituents of the target (sphere and plane) plus some new resonances due to the coupling between them. Some are below the excitation energy in the isolated particle, around 6.8 and 7.8 eV, and the others (dimer ones) are above the planar surface plasmon energy. From these resonances, the peak around 6.8 eV is of special interest. It is almost the same intensity as the dipolar mode in the isolated sphere (at $\omega_p/\sqrt{3}$), which lies around 8.7 eV. The energy of the new resonance at 6.8 eV does not depend on the sphere radius or the relative position of the electron and target, but its intensity is a maximum for the case considered.[44] The behavior of this peak at 6.8 eV as a function of the impact parameter (represented in Fig. 3) is similar to that of the dipolar term in the isolated sphere. We find the expected impact parameter dependence $P(\omega)\sim e^{-2\omega/v}$, concluding that the spatial resolution of the energy-filtered images at 6.8 eV is $\sim(v/2\omega)$.

It should be noticed that, for trajectories very close to the sphere, the solution of system (12) in the region of 8–10 eV is not quite stable; some small shifts in the energy of the peaks are produced, depending on the parity of the maximum value of l considered when solving system (12). Nevertheless, around the peaks of 6.8 and 10.7 eV the solution is quite stable even if only a few terms are considered. The origin of such instabilities can be attributed to the use of polar coordinates to describe the excitations in the planar interface, as has been done in this work, and to the use of a Drude dielectric function with very small damping. Working with experimental dielectric functions, as we do in the following cases, this problem does not appear. In any case the instabilities are not physically relevant, and are to be studied in more detail in a work in progress.

In Fig. 2(b) we have plotted the calculated spectra for two trajectories, corresponding to $\theta_0=60°$ and 85°, denoted by C and B, respectively. Comparing these results with those of Fig. 2(a) it is seen that the negative correction around ω_s is more important as the electron trajectory is closer to the planar interface. Another point is the fact that, as the electron trajectory is moved from the top of the particle toward the edge, the probability distributes in such a way that the peaks for $\omega<\omega_s=10.7$ eV decrease in intensity as the probability for $\omega>\omega_s$ increases. For trajectories close to the sphere-plane edge, the spectrum is consistent with the modes of a particle traveling close to one edge.[53]

Batson[10,21] measured electron energy losses in the range 3–4 eV in systems consisting of a small Al ($a\sim10$ nm) sphere supported on a larger one, with a resolution in energy of 1 eV. However, those resonances were not present in the spectra obtained near an isolated particle. On the other hand, he observed that particular resonance for trajectories over the top of the small sphere, but not when the electron passes near the edge between the small and large particles. Our results shown in Fig. 2 are in qualitative agreement with Batson's measurements.

A simple way of studying the effect of an oxide coating in the target is to consider that the outer medium is alumina, as proposed by Schmeits and Dambly.[34] In Fig.

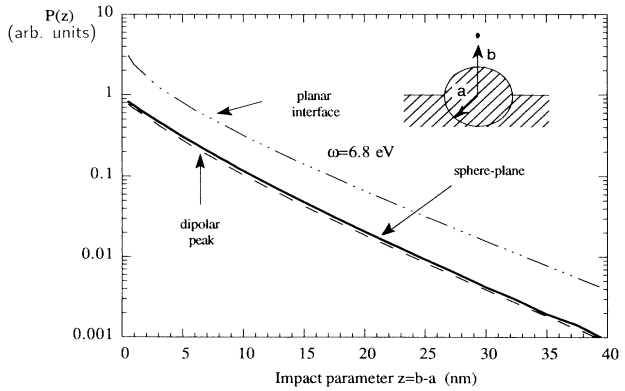

FIG. 3. Intensity of the $\omega=6.8$ eV resonance as a function of the impact parameter $z=b-a$ for an Al particle on an Al support (continuous line). The electron trajectory passes over the top of the particle ($\theta_0=0$). The probabilities corresponding to the dipolar peak of the isolated sphere (dashed line) and to the planar interface (dash-dotted line) have also been plotted for two metals having their corresponding surface plasmons at 6.8 eV.

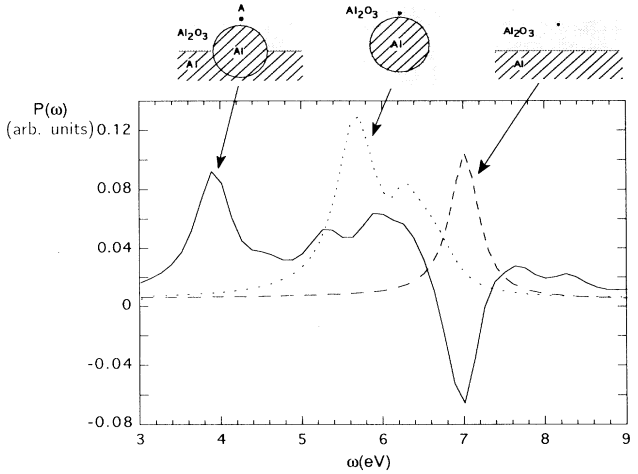

FIG. 4. Calculated spectra corresponding to an Al sphere of radius $a=10$ nm, half embedded in an Al-Al_2O_3 interface (continuous line). The electron trajectory (A) corresponds to impact parameter $b=11$ nm. The spectra of an Al sphere in an Al_2O_3 (dotted line) infinite medium and Al-Al_2O_3 interface (dashed line) for length $2a$, for the same impact parameters, have also been plotted.

4 we have considered the same case as Fig. 2, that is the Al sphere on an Al support, but now the upper medium has been filled with aluminum oxide. The spectra corresponding to the isolated sphere in oxide and the corresponding planar interface have also been plotted for comparison. The effect of the alumina is to soften the peaks and to displace them toward lower energies. The first peak, located below the excitations associated with the isolated sphere, appears at energies lower than 4 eV. This result is consistent with the experimental results reported by Batson and mentioned above.

Wang and Cowley[30–32] obtained EELS spectra with 1-eV energy resolution near Al particles partially embedded in AlF_3. They observed surface plasmon excitations around 4 and 7–8 eV. In Fig. 5 we have considered that problem, i.e., now the support has been replaced by AlF_3 instead of Al. To compute the dielectric response functions, experimental optical data have been used in the case of Al,[54] and data from EELS experiments for AlF_3.[55] Spectra for the same trajectories A and B as in the previous figures have been calculated and compared with those for the same impact parameter, but near an isolated sphere in vacuum and when it is fully introduced in an AlF_3 matrix. The sphere radius is $a=10$ nm, and the distance from the incident electron to the sphere center is $b=11$ nm. Now the spectra near the half-embedded sphere are rather a distortion of those corresponding to isolated spheres. For trajectory A, the spectrum is very close to that of the Al sphere in vacuum, but the intensity at the energy of the dipolar mode (around 8.5 eV) is reduced and another excitation appears around 7 eV, the excitation corresponding to the isolated sphere immersed in AlF_3. For trajectory B, the spectrum looks like that of the isolated sphere in AlF_3, but it is slightly displaced toward higher energies (toward the excitation of the isolated sphere in vacuum) and presents another maximum around 10 eV.

Similar experiments with Si particles have been reported by Ugarte, Colliex, and Isaacson,[24] in which they measured a surface-mode excitation at 3–4 eV. In Fig. 6 we present the results for a particle of amorphous Si half embedded into a support of the same material for a trajectory of type A. Now the sphere radius is 12 nm, and the distance from the electron to the sphere center $b=13$ nm. We have plotted the spectra corresponding to the Si isolated sphere and the Si-vacuum interface separately for the same impact parameter. The Si dielectric response function has been obtained from optical data available in the literature.[56] For the infinite planar interface, we have plotted the energy-loss probability corresponding to a trajectory interval of $2a$ length. The main feature to be underlined in the case of the embedded Si sphere, with respect to the isolated one, is the decrease in intensity of the excitations around 9.5 eV, and the emergence of a broad peak around 7.5 eV. These values are above the 3–4 eV surface excitations measured by Ugarte, Colliex, and Isaacson in silicon particles. In our model, a displacement of the excitation toward lower energy is obtained by considering the oxide in the upper region.

In practice, the aluminum small particles usually appear oxidized. We have studied the effect of the oxide coating on the energy-loss spectrum of an Al particle half embedded in an Al planar interface, by numerically computing expressions (15) and (17). As can be noticed, the oxide coating reduces the coupling between the metallic particle and the support. In Fig. 7(a) we have plotted the energy loss corresponding to a supported particle of radius 10 nm with a thin oxide coating layer of 1-nm width. The electron trajectory passes over the top of the sphere, at a distance from the particle outer surface of $b-a_2=1$ nm. In the same plot the spectrum of the same isolated particle and the same electron trajectory has been shown for comparison. The coupling sphere support gives rise to the new resonance at 6.8 eV, and a lowering of the surface excitation corresponding to the isolated oxidized

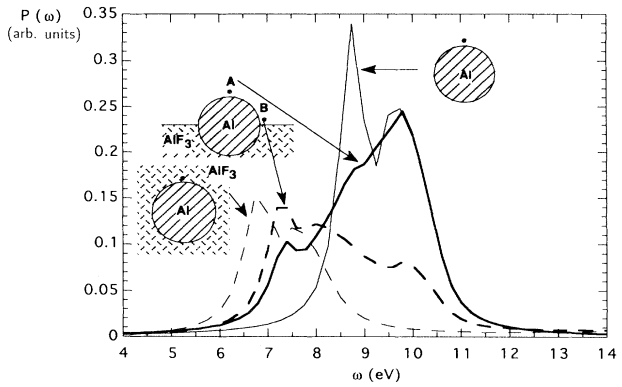

FIG. 5. Excitation probabilities corresponding to an electron traveling near an Al particle half embedded in an AlF_3-vacuum interface (wide line) for trajectories A (continuous line) and B (wide dashed line). The probabilities corresponding to an isolated Al sphere in a vacuum (continuous line), and the AlF_3 (dashed line), have also been plotted. The particle radius is $a=10$ nm, and the impact parameter $b=11$ nm.

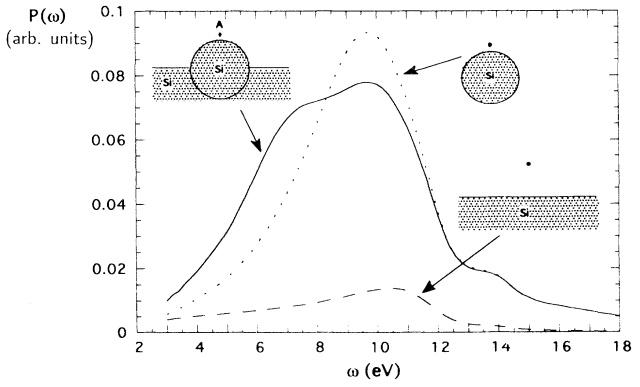

FIG. 6. Excitation probability vs energy ω for an electron traveling near a Si particle half embedded in a Si-vacuum planar support, along the trajectory marked as A (continuous wide line). The particle radius is $a=12$ nm, and the electron impact parameter $b=13$ nm. The probabilities corresponding to a planar Si-vacuum interface for length $2a$ (dashed line) and an isolated Si particle (dotted line) have also been plotted. 50 terms have been considered in the series.

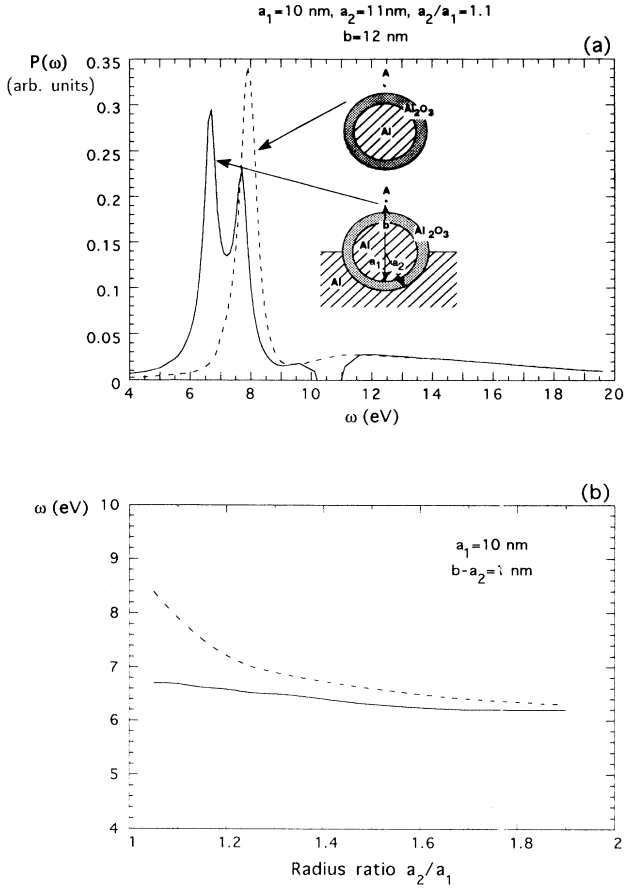

FIG. 7. (a) Energy-loss probability for an electron traveling along trajectory A ($\theta_0=0$, $b=12$ nm) over a half-embedded oxidized Al particle (continuous line) and an isolated particle (dashed line) for the same inner and outer particle radii, $a_1=10$ nm and $a_2=11$ nm. (b) Dependence of the energy of the isolated oxidized particle resonance (dashed line) and the lower peak energy of the supported oxidized particle spectrum (continuous line) with the oxide coating thickness (ratio between both radii a_2/a_1). The inner radius $a=10$ nm, as well as the distance from the electron to the outer surface, $b-a_2=1$ nm, have been kept constant.

sphere at around 8 eV. The correction to the energy loss in an infinite planar interface due to the presence of the particle gives rise to negative values of the probability around 10.7 eV, as in the clean particle case. As the coating becomes thicker, the peaks move toward lower values of energy, especially the peak at 7.5–8 eV, in such a way that both peaks mix up and the spectra of the isolated particle and the supported particle become the same. The displacement of those peaks as a function of the coating thickness (the ratio between the radii, a_2/a_1) has been plotted in Fig. 7(b).

IV. CONCLUSIONS

In conclusion, we have obtained an expression of the energy-loss probability useful in most cases of interest in EELS experiments in STEM, especially when complex targets are involved. The expression has been computed to evaluate the energy loss near a spherical particle coupled to a planar interface and half embedded in it. For metallic Al particles half embedded in Al, the coupling between the sphere and the support gives rise to different resonances below and above the isolated-sphere energy excitations, the most important being around 6.8 eV. For nonconducting supports, as in the case of AlF_3 or Si, the coupling sphere support is not so important; only a slight distortion of the isolated sphere spectrum is found due to the presence of the support. For oxide-coated 10-nm Al particles the effect of the support (giving rise to a new resonance around 6.8 eV) would be observable only for a coating thickness larger than around 2 nm, provided a resolution of 1 eV is available.

ACKNOWLEDGMENTS

The authors wish to acknowledge Dr. C. M.M. Nex for his advice on the numerical resolution, and Professor P. M. Echenique, Professor E. Zaremba, and Professor R. H. Ritchie for their stimulating discussions. They also thank the Basque Country Government (project PGV9114.1), Gipuzkoako Foru Aldundia and Iberdrola for financial help, and Labein for the use of computing facilities.

[1]F. Fujimoto, K. Komaki, and K. Ishida, J. Phys. Soc. Jpn. **23**, 1186 (1967).
[2]A. A. Fujimoto and K. Komaki, J. Phys. Soc. Jpn. **25**, 1679 (1968).
[3]P. E. Batson, Solid State Commun. **34**, 477 (1980).
[4]P. E. Batson and M. M. J. Treacy, in *Proceedings of the 40th ESMA Meeting*, edited by G. W. Bailey (San Francisco Press, San Francisco, 1980), p. 126.
[5]A. Howie and R. H. Milne, Ultramicroscopy **18**, 427 (1985).
[6]L. D. Marks, Solid State Commun. **43**, 727 (1982).
[7]T. L. Ferrell and P. M. Echenique, Phys. Rev. Lett. **55**, 1526 (1985).
[8]P. M. Echenique, J. Bausells, and A. Rivacoba, Phys. Rev. B **35**, 1521 (1987).
[9]P. M. Echenique, A. Howie, and D. J. Wheatley, Philos. Mag. B **56**, 335 (1987).
[10]P. E. Batson, Ultramicroscopy **9**, 277 (1982).
[11]S. Munnix and M. Schmeitz, Phys. Rev. B **32**, 4192 (1985).
[12]T. L. Ferrell, R. J. Warmack, V. E. Anderson, and P. M. Echenique, Phys. Rev. B **35**, 7365 (1987).
[13]J. Bausells, A. Rivacoba, and P. M. Echenique, Surf. Sci. **189/190**, 1015 (1987).
[14]R. Ruppin, J. Phys. Chem. Solids **39**, 233 (1978).
[15]N. Barberán and M. Battle, J. Phys. C **20**, 3583 (1987).
[16]A. D. Boardman and B. V. Paranjape, J. Phys. F **7**, 1935 (1977).
[17]B. Dasgupta and R. Fuchs, Phys. Rev. B **35**, 3722 (1987).
[18]E. Zaremba and B. N. J. Persson, Phys. Rev. B **35**, 596 (1987).
[19]R. Fuchs and F. Claro, Phys. Rev. B **35**, 3722 (1987).
[20]R. Rojas, F. Claro, and R. Fuchs, Phys. Rev. B **37**, 6799 (1988).
[21]P. E. Batson, Phys. Rev. Lett. **49**, 936 (1982).

[22]D. Ugarte, C. Colliex, and P. Trebbia, in *Proceedings of the 12th Werner Brandt International Conference, San Sebastian 1989,* edited by R. H. Ritchie and P. M. Echenique (Oak Ridge National Laboratory, Tennessee, 1990), p. 25.
[23]D. Ugarte, Thèse, Université de Paris-Sud, 1990.
[24]D. Ugarte, C. Colliex, and P. Trebbia, Phys. Rev. B **45**, 4332 (1992).
[25]M. Scheinfein and M. Isaacson, Ultramicroscopy **16**, 233 (1985).
[26]A. Howie and C. A. Walsh, Microsc. Microanal. **2**, 171 (1991).
[27]D. Stroud and F. P. Pan, Phys. Rev. B **17**, 1602 (1978).
[28]A. Wachniewski and H. B. Mc. Clung, Phys. Rev. B **33**, 8053 (1986).
[29]Z. L. Wang and J. M. Cowley, Ultramicroscopy **21**, 77 (1987).
[30]Z. L. Wang and J. M. Cowley, Ultramicroscopy **21**, 335 (1987).
[31]Z. L. Wang and J. M. Cowley, Ultramicroscopy **21**, 347 (1987).
[32]Z. L. Wang and J. M. Cowley, Ultramicroscopy **23**, 97 (1987).
[33]J. S. Nkoma, Surf. Sci. **245**, 207 (1991).
[34]M. Schmeits and L. Dambly, Phys. Rev. B **44**, 12 706 (1991).
[35]M. Schmeits, Phys. Rev. B **39**, 7567 (1989).
[36]N. Zabala and A. Rivacoba, Ultramicroscopy **35**, 145 (1991).
[37]N. Zabala and P. M. Echenique, Ultramicroscopy **32**, 327 (1990).
[38]L. D. Landau and E. M. Lifshitz, *Quantum Mechanics, Course of Theoretical Physics* (Pergamon, Oxford, 1977), Vol. 3, p. 146.
[39]R. H. Ritchie, Phys. Rev. **106**, 874 (1957).
[40]P. M. Echenique and J. B. Pendry, J. Phys. C **8**, 2936 (1975).
[41]P. M. Echenique, R. H. Ritchie, L. Barberán, and L. J. C. Inkson, Phys. Rev. B **23**, 6485 (1981).
[42]C. A. Walsh, Philos. Mag. A **59**, 227 (1989).
[43]N. Zabala, A. Rivacoba, and P. M. Echenique, Surf. Sci. **209**, 465 (1989).
[44]A. Rivacoba, N. Zabala, and P. M. Echenique, Phys. Rev. Lett. **69**, 3362 (1992).
[45]L. Hedin and S. Lundquist, *Solid State Physics,* edited by H. Ehrenreich and D. Turnbull (Academic, New York, 1969), Vol. 27, p. 1.
[46]J. R. Manson and R. H. Ritchie, Phys. Rev. B **34**, 4867 (1981).
[47]R. H. Ritchie, Philos. Mag. A **44**, 931 (1981).
[48]R. H. Ritchie and A. Howie, Philos. Mag. A **58**, 753 (1988).
[49]E. Zaremba, Surf. Sci. **151**, 91 (1985).
[50]Lord Rayleigh, Philos. Trans. **CLX**, 579 (1870).
[51]I. S. Gradshteyn and I. M. Ryzhik, *Table of Integrals, Series and Products* (Academic, New York, 1980), p. 795.
[52]C. M. M. Nex and R. G. Wolley, J. Phys. C **18**, 2955 (1985).
[53]R. Garcia-Molina, A. Gras-Marti, and R. H. Ritchie, Phys. Rev. B **31**, 121 (1985).
[54]H. J. Hagemann, W. Gudat, and C. Kunz, Desy Report SR74/7 (1974) (unpublished).
[55]C. A. Walsh, Ph.D. Thesis, University of Cambridge (1989).
[56]*Handbook of Optical Constants of Solids,* edited by E. D. Palik (Academic, London, 1985).